PCCP

PAPER

View Article Online
View Journal | View Issue

Cite this: *Phys. Chem. Chem. Phys.*, 2014, **16**, 26176

First principles study of point defects in SnS†

Brad D. Malone,*[a] Adam Gali[bc] and Efthimios Kaxiras[ad]

Received 9th July 2014,
Accepted 22nd October 2014

DOI: 10.1039/c4cp03010a

www.rsc.org/pccp

Photovoltaic cells based on SnS as the absorber layer show promise for efficient solar devices containing non-toxic materials that are abundant enough for large scale production. The efficiency of SnS cells has been increasing steadily, but various loss mechanisms in the device, related to the presence of defects in the material, have so far limited it far below its maximal theoretical value. In this work we perform first principles, density-functional-theory calculations to examine the behavior and nature of both intrinsic and extrinsic defects in the SnS absorber layer. We focus on the elements known to exist in the environment of SnS-based photovoltaic devices during growth. In what concerns intrinsic defects, our calculations support the current understanding of the role of the Sn vacancy (V_{Sn}) acceptor defect, namely that it is responsible for the p-type conductivity in SnS. We also present calculations for extrinsic defects and make extensive comparison to experimental expectations. Our detailed treatment of electrostatic correction terms for charged defects provides theoretical predictions on both the high-frequency and low-frequency dielectric tensors of SnS.

I Introduction

Tin sulfide (SnS) has emerged as an interesting candidate for efficient absorber material in photovoltaics because it fulfills several crucial requirements for large-scale production:[1–6] it has strong absorption near the optical absorption edge of ~1.3 eV,[1,7] it is stable in the presence of water and oxygen,[8] and it is made out of abundant and non-toxic elements.[9] Devices based on SnS as the absorber currently exhibit efficiencies much less than the theoretical maximal efficiency of ~25%;[2,8] the record efficiency currently realized for a SnS-based device is only around 4.4%.[8] However, the efficiencies have been climbing rapidly, more than tripling in the past two years.[4,8] This rapid advancement is cause for optimism that further increases are possible if the various loss mechanisms can be controlled.

Much of the recent progress in increasing the efficiency of SnS-based devices is due to the reduction of interface recombination. This was achieved through enlarged grain sizes and through the adjustment of neighboring materials in order to optimize the band offsets.[2,8,10] Further improvements along these lines are being pursued, including theoretical work on band offsets.[11,12] A different approach for optimizing device performance is to understand the role of defects in SnS. This understanding is crucial in assisting experimental efforts to optimize the preparation conditions and to clarify whether the materials used in the preparation or the interfaces themselves introduce defects detrimental to device performance.

The aim of this work is to employ first-principles density functional theory (DFT) calculations to investigate a large number of point defects which could potentially affect the properties of SnS and limit its photovoltaic potential. Vidal *et al.*[13] recently carried out a first-principles study of the intrinsic defects, vacancies, self-interstitials, and antisites. We extend this study by examining potential dopants of SnS. These include the group-V elements N, P, As, and Sb, as well as elements that are of interest because of their doping properties or because of their presence at the interfaces of the SnS absorber or in the preparation environment, namely, O, Cl, Cu, Na, In, Cd, and Zn. For each of these elements we evaluate the stability in both Sn and S substitutional positions as well as in interstitial sites.

II Methods

Our DFT calculations are performed using the plane-wave projector augmented-wave (PAW) method as implemented in the VASP code,[14–16] with the Perdew, Burke, and Ernzerhof (PBE) functional for exchange and correlation.[17] We explicitly include the Sn d-electrons in the valence manifold, and use a

[a] *School of Engineering and Applied Sciences, Harvard University, Cambridge, MA, 02138, USA. E-mail: brad.malone@gmail.com*
[b] *Institute for Solid State Physics and Optics, Wigner Research Centre for Physics, Hungarian Academy of Sciences, Budapest, POB 49, H-1525, Hungary*
[c] *Department of Atomic Physics, Budapest University of Technology and Economics, Budafoki út 8, H-1111, Budapest, Hungary*
[d] *Department of Physics, Harvard University, Cambridge, MA, 02138, USA*

† Electronic supplementary information (ESI) available. See DOI: 10.1039/c4cp03010a

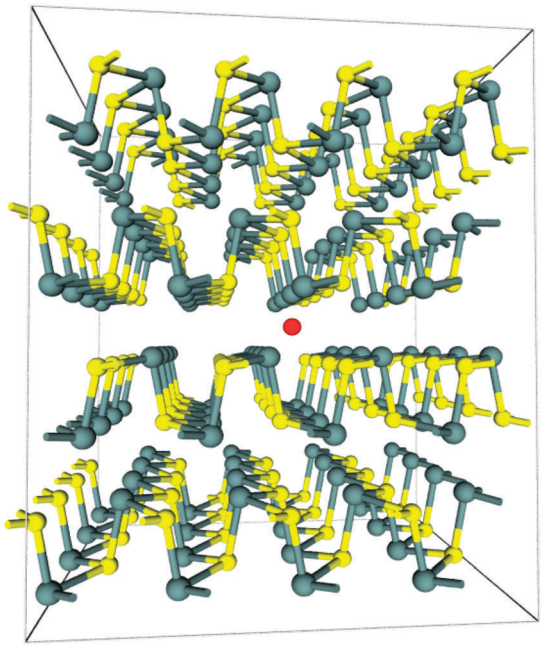

Fig. 1 The SnS supercell, outlined in black lines and containing a total of 256 bulk atoms, used for the calculation of the defect formation energies. Sn atoms are shown in gray, S in yellow, and the site of the interstitial defect is shown in red.

450 eV energy cutoff for the wavefunction expansion in order to get well-converged energies and forces. Using these parameters, we obtain lattice constants of SnS of a = 4.42 Å, b = 4.03 Å, and c = 11.41 Å, which are in good agreement with the experimental values of a = 4.334 Å, b = 3.987 Å, and c = 11.20 Å.[18,19] The band gap of the relaxed SnS structure is found to be indirect, at 0.90 eV, which underestimates the zero-temperature band gap of $\sim$1.25 eV,[11] as expected for DFT calculations.

In order to evaluate defect formation energies and minimize spurious defect–defect interactions, we construct large 256-atom supercells of SnS that gives a reasonable approximation of the isolated defects. The supercell, shown in Fig. 1, corresponds to a $4 \times 4 \times 2$ multiple of the 8-atom primitive SnS unit cell. We sample the Brillouin zone of the supercell with a fine grid of $2 \times 2 \times 2$ divisions rather than using the Γ point only as is typical in other calculations due to the computational expense. The formation enthalpy $E_f(D,q)$ of a defect D in charge state q is given by

$$E_f(D,q) = E_{tot}(D,q) - E_{tot}(0) - \sum_i n_i\mu_i + q(E_{VBM} + E_F + \Delta V) \quad (1)$$

where $E_{tot}(D,q)$ and $E_{tot}(0)$ are the total energies of the supercell with and without the defect.[20] The defect is created by adding or removing n_i atoms with chemical potentials μ_i from the defect-free "pure" supercell. E_F is the Fermi level referenced to the valence band maximum, E_{VBM}, in the defect-free cell. Because the VBM is referenced to the pure cell, an alignment term ΔV is added to align the electrostatic potentials between the defect and the pure cells. In the present calculations this term is taken as the difference in electrostatic potentials between the atomic site furthest from the defect in the defect supercell with its equivalent site in the defect-free cell.[21] The choice of chemical potentials is important in order to give realistic estimates of the formation enthalpies, and are restricted by values required to maintain a stable host compound and to avoid the precipitation of competing phases of Sn–S or those that can be formed from the host atoms and the dopants.[22] Conventionally, the chemical potentials are referenced to their bulk phase, that is, $\mu_i = \mu_i^{bulk} + \Delta\mu_i$, and the above constraints impose conditions on the allowed values of $\Delta\mu_i$. For example, in order to prevent precipitating the bulk solid we must have $\Delta\mu_i \leq 0$. Furthermore, in order to maintain a stable SnS compound the chemical potentials for Sn and S must satisfy the equation

$$\mu_{Sn} + \mu_S = \Delta H(SnS) + \mu_{Sn}^{bulk} + \mu_S^{bulk} \quad (2)$$

or equivalently

$$\Delta\mu_{Sn} + \Delta\mu_S = \Delta H(SnS) \quad (3)$$

where ΔH(SnS) is the heat of formation of SnS.

For the competing phases of SnS, such as SnS_2 or Sn_2S_3, we impose constraints on the chemical potentials of the type

$$m\Delta\mu_{Sn} + n\Delta\mu_S \leq \Delta H(Sn_mS_n) \quad (4)$$

Finally, in order to put reasonable limits on the chemical potentials of the extrinsic defects, we consider restrictions that not only prevent precipitation of the bulk phases of the dopant, but also prevent formation of phases of the dopant and the host atoms. For example, for Zn defects, $\Delta\mu_{Zn}$ is restricted by the condition that ZnS does not form:

$$\Delta\mu_{Zn} + \Delta\mu_S \leq \Delta H(ZnS) \quad (5)$$

We considered a large number of possible phases which the dopant atoms might form with the host atoms to set proper limits on the values of the dopant chemical potentials: ZnS, CdS, NaSn, NaS, Na_2S_2, AsS, SnAs, P_4S_3, SnP_3, Sb_2S_3, SnSb, SnO_2, CuS, $Cu_{20}Sn_6$, SCl_2, $SnCl_4$, and $SnCl_2$. The computed total energies of all these phases are implicitly contained in the formation energies of the defects that we present below, through their effect on the chemical potentials.

Despite the use of large supercells to model the isolated defect, the calculation of charged defect levels is problematic because of the long-range nature of the Coulomb interaction, resulting in very slow convergence of the spurious electrostatic interactions between the defect and its periodic images.[23,24] Existing schemes that attempt to correct this problem are based on the assumption that the dielectric screening in the material is isotropic. SnS is not a cubic material and its dielectric properties cannot be simply described by a single dielectric constant ε. The high-frequency dielectric constant is only slightly anisotropic and thus might reasonably be approximated by a single value. The situation is more complicated for the low-frequency dielectric constant which includes the effects of screening from the ionic relaxation.[25] It is this latter dielectric constant which should be applied in the event that full relaxation is taken into account for in

the supercell calculations of the defect.[26] Accordingly, proper treatment of the anisotropic nature of the screening should be included in the electrostatic correction. A new method has been proposed recently to deal with anisotropic screening in the calculation of defect formation energies by incorporating the dielectric *tensor* into the determination of the Madelung potential. This gives rise to a screened Madelung potential which can be used to correct finite-size defect formation energies to the infinite-size limit.[27] In our work we use this method, wherein the defect formation energies for the 256-atom defect-containing supercell are corrected using an Ewald-type correction, obtained from the Madelung potential with the low-frequency dielectric tensor of the defect-free SnS system. This results in a correction of 32 meV $\times q^2$ being applied to the formation energy of each defect with charge q. While this treats the anisotropic nature of the screening correctly, it approximates the screening near the defect as being unmodified from the pure crystal case. This can be improved by fitting the dielectric tensor using a range of different defect supercell sizes.[27] We do not pursue this more elaborate treatment here because of the very high computational cost involved in doing a large number of supercell sizes for all of the defects we examined.

Finally, as noted above, the DFT calculations underestimate the experimental band gap of 1.25 eV by about 0.35 eV. Methods beyond DFT that could improve on the description of the electronic structure are computationally too expensive to pursue here. This leads to an ambiguity in how the formation enthalpy and charge transition levels should be plotted as a function of the Fermi energy, which varies from the valence band maximum to the conduction band minimum. In our calculations we adopt the "extended gap scheme",[28] namely, we plot the defect formation enthalpies up to the experimental gap of 1.25 eV. It should be noted that the resulting formation energies and charge transition levels can be affected by the use of standard DFT exchange–correlation functionals, and important corrections can sometimes result in going to more accurate treatments such as quasiparticle approaches based on the GW approximation.[29] An example of these differences can be seen in the work of ref. 30 in which this was studied in detail for the Si self-interstitial defect.

III Results

A. Dielectric tensor

In order to obtain the dielectric tensor needed to construct the electrostatic corrections, we perform density functional perturbation theory calculations on the pure crystal SnS, which allows for both the calculation of the high-frequency (with fixed ions) dielectric tensor, ε_∞, as well as the low-frequency (relaxed ionic positions) dielectric tensor, ε_0.[31,32] In these calculations local-field effects have been taken into account including both Hartree and exchange–correlation contributions.

The results of the calculations are presented in Table 1, and compared to experiment. The dielectric tensor for SnS is diagonal and thus we present the results in terms of the components corresponding to the principal directions parallel to the lattice vectors (see Section II for the lattice orientation). The calculated results for both ε_0 and ε_∞ are in good agreement with the experimental values obtained from infrared reflectivity measurements and high-resolution electron-energy-loss spectroscopy.[25,33,34] In particular, for the component with the most uncertainty in the experimental data, $\vec{E}\|\vec{b}$, the results calculated in this work fall in the middle of the range spanned by the experimental values.

Table 1 Comparison of the low-frequency (ε_0) and high-frequency (ε_∞) dielectric constants calculated in this work with experimental results

	ε_0			ε_∞		
$\vec{E}\|\|$	$\vec{a}$	$\vec{b}$	$\vec{c}$	$\vec{a}$	$\vec{b}$	$\vec{c}$
This work	28.5	40.4	25.6	13.2	15.0	13.2
Ref. 25	29	38	33	14	19	14
Ref. 33	32	48	32	14	16	17
Ref. 34	32.4	48.4	32.3	11.7	13.9	12.8

B. Intrinsic defects

We first consider the formation enthalpies of intrinsic defects, namely Sn or S vacancies, antisites, and interstitials. The results of these calculations are presented in Fig. 2. Experimentally, SnS is almost always p-type,[3,35,36] which has been explained by previous theoretical work as being due to Sn vacancies which show an acceptor-like behavior.[13] This result is consistent with the present calculations, especially in the S-rich limit, as the V_{Sn} defect has a very low formation enthalpy which even becomes negative at a Fermi energy of approximately 0.7 eV. Above this value, Sn vacancies would spontaneously form, introducing holes into the system and pulling the Fermi energy down to lower values. In the S-rich limit, for very low values of the Fermi energy, the sulfur vacancy has lower formation enthalpy than V_{Sn}. This defect acts as a donor, introducing electrons into the system and raising the Fermi energy. While the equilibrium

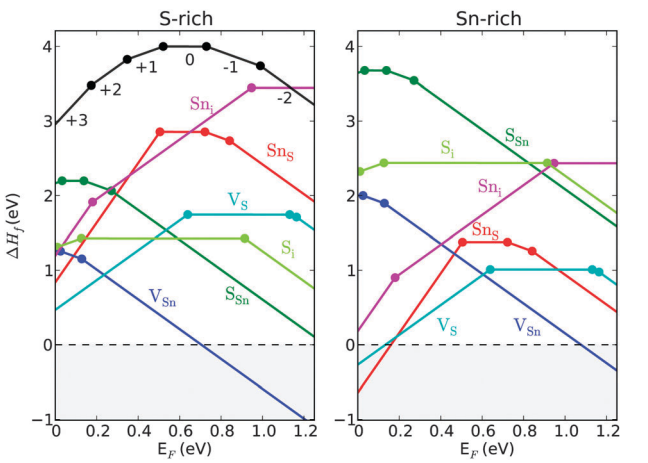

Fig. 2 Calculated defect formation enthalpies for the intrinsic defects under S-rich (left) and Sn-rich (right) conditions. The black segments near the top of the S-rich panel, labeled +3, +2, +1, 0, −1, −2, illustrate how the charge of the defect at a particular position of the Fermi energy can be inferred from the slope of the formation enthalpy at that position.

Fermi energy should in principle be determined by a self-consistent solution depending upon the system temperature, including effects of the free carriers and all relevant defects, it should remain close to the intersection of $\Delta H_f(V_S^{++}) = \Delta H_f(V_{Sn}^{--})$. Deviations from this point will be compensated by the increasing relative concentrations of one of these defects, pushing the Fermi energy back towards this point. In our calculations this intersection occurs at E_F = 0.24 eV, which is very close to the experimentally reported value of 0.28 eV.[10] Despite this seemingly good agreement, we caution that it is difficult to establish at which point within the range of allowed chemical potential values the experimental growth and measurements are obtained.

In the Sn-rich limit, donor defects such as Sn_i, Sn_S, and V_S become energetically favorable at low values of the Fermi energy, as seen from Fig. 2. This will tend to push the Fermi energy to higher values in the band gap and decrease the hole concentration. This behavior is consistent with the experimental finding that the hole concentration drops with increasing temperature, which is associated with S-poor conditions because of the volatility of sulfur.[13]

We comment here on the differences between our results with those obtained in recent theoretical work on the intrinsic defects in ref. 13, based on the same methodology. While the overall picture is similar, especially in what concerns the V_{Sn} defect which gives rise to the p-type nature of the material, there are a number of differences, in particular on the specific charge states which are stable and the value of the Fermi energy at which the transitions from one charge state to another occur. These differences can be ascribed to the various approximations involved in the two sets of calculations, in particular the choice of exchange–correlation functional, the size of the supercell, the treatment of the electrostatic corrections, and the treatment of the interlayer spacing. The results presented here are obtained with the GGA functional, whereas those of ref. 13 utilized the LDA functional. Our calculations are performed with larger 256-atom supercell in comparison to the 72-atom supercell of ref. 13. As discussed in Section II, we employ a recent electrostatic scheme that accounts for the anisotropy of the dielectric tensor. It is possible that in ref. 13 this anisotropy was not taken into account and it is unclear which dielectric constant (high-frequency of low-frequency) was used in the correction scheme. These aspects are likely to be of increasing importance in the calculations using a smaller supercell. Finally, in ref. 13 it is noted that some defect enthalpies depend sensitively on the interlayer distance. A case in point is the relaxation effect of the 2+ charge state of V_S, in which a Sn atom that has lost one of its S bonding neighbors relaxes into the interlayer space, and is affected by the size of this space. We find similar effects. In order to take this into account, in our calculations we fully relax all atomic positions, including the interlayer spacing, whereas in ref. 13 the interlayer spacing was held fixed to the experimental value while the other structural parameters are relaxed.[37] In our defect calculations, the supercell lattice parameters are held to their bulk values.

C. Group V defects: P, N, As, Sb

We turn next to extrinsic defects that may be present in the SnS system, focusing first on group V elements. The majority of these elements have been found as impurities in SnS samples in past experimental work or have been introduced deliberately in an attempt to modify the properties of the host material. The defect formation enthalpies of the group IV elements are presented in Fig. 3 and 4 in the S-rich and Sn-rich limits.

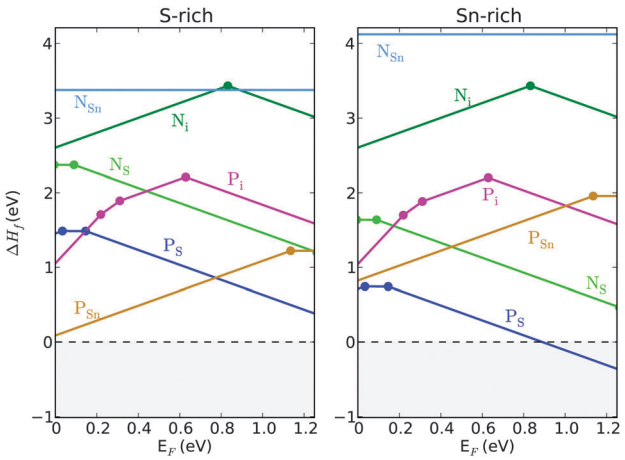

Fig. 3 Calculated defect formation enthalpies for extrinsic defects formed from the group V elements P and N, under S-rich (left) and Sn-rich (right) conditions.

Yue *et al.* have reported the fabrication of doped p–n homojunction SnS nanowire arrays using P as an electron donor when occupying the Sn site.[5] This is an interesting result, as n-type SnS has only rarely been reported, and most previous work attempting to create n-type SnS using other dopants has failed.[35] The creation of n-type SnS, especially if it could be reproduced in thin films, would allow for the creation of SnS homojunctions. This might be beneficial to efficiency, by preventing some of the losses that are present at the hetero-interfaces. The occupation of Sn sites by P is counter-intuitive, due to the similarity of P with S which suggest that P would prefer to occupy the S sites. Our results show that the site preference for P depends strongly on the environmental conditions.

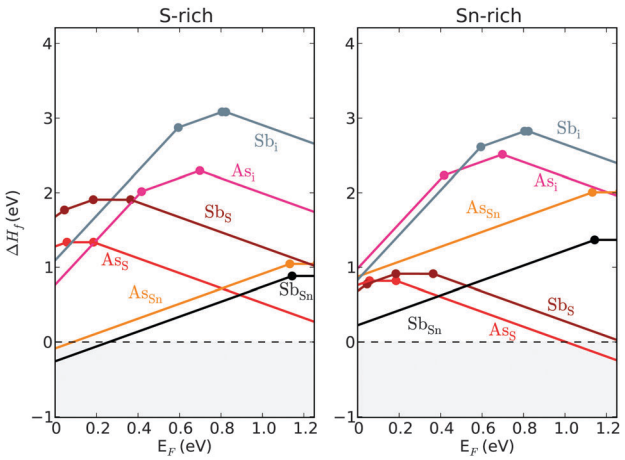

Fig. 4 Calculated defect formation enthalpies for extrinsic defects formed from the group V elements As and Sb, under S-rich (left) and Sn-rich (right) conditions.

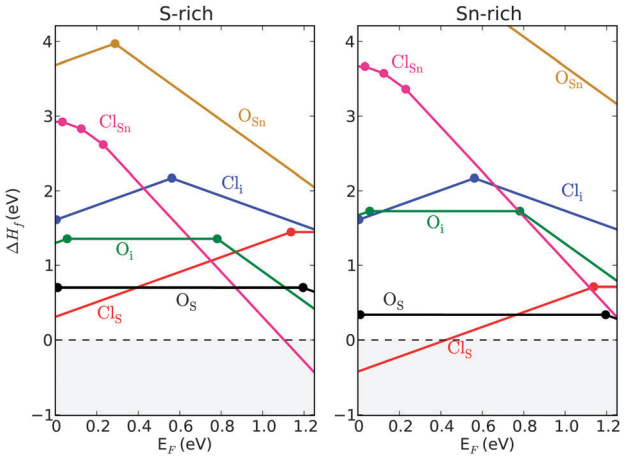

Fig. 5 Calculated defect formation enthalpies for extrinsic defects formed from the elements Cl and O, under S-rich (left) and Sn-rich (right) conditions.

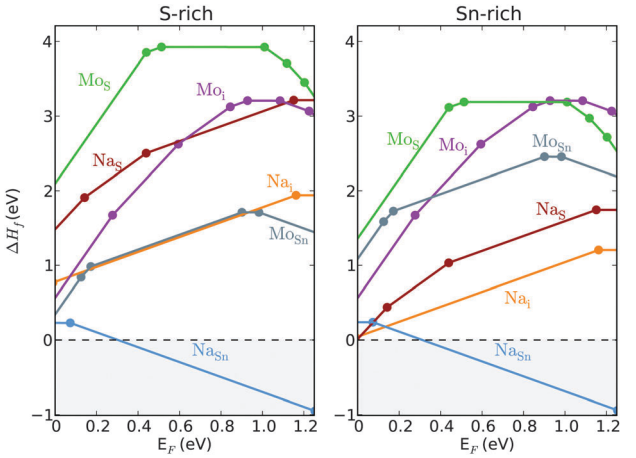

Fig. 6 Calculated defect formation enthalpies for extrinsic defects formed from the elements Na and Mo, under S-rich (left) and Sn-rich (right) conditions.

In particular, under S-rich conditions, P prefers to occupy the Sn sites, where it acts as an electron donor, with a very low formation enthalpy. However, under Sn-rich conditions, the P_S defect becomes more favorable, which would act as acceptor.

N is often used to assist the SnS growth process,[35] and has been found to increase the p-type character of SnS.[38] We find that, regardless of the environmental conditions, N is unlikely to occur either as an interstitial or as a substitutional defect at the Sn site. Furthermore, N_{Sn} is electrically neutral and exhibits no transitions between charge states within the band gap. Even the N_S defect is energetically unfavorable over a large of Fermi energy values. However, in agreement with the experimental results, it does act as a shallow acceptor and would increase the p-type conductivity.

Sb is found as an impurity in SnS samples,[36] and has been used as n-type dopant of SnS.[35] Experimentally, Sb acting as an n-type dopant compensates holes in SnS,[36] and is incorporated under S-rich conditions as Sb_{Sn}.[35] Our calculated results shown in Fig. 4 support these experimental facts. We find that the Sb_{Sn} defect forms readily, with negative formation enthalpy at low values of the Fermi energy in S-rich conditions and acts as a donor, explaining its ability to make the SnS less p-type. As the environmental conditions shift towards Sn-rich, the formation enthalpy of the Sb_S defect becomes comparable to that of Sb_{Sn}. The Sb_S defect acts as an acceptor under a wide range of Fermi energy values, limiting the ability of Sb to drive the SnS toward n-type behavior.

In what concerns As, we are not aware of any experimental reports of its use in SnS samples. Our results suggest that As in SnS behaves similar to Sb: the formation enthalpies and the electronic transitions are similar to those of Sb, for both types of substitutional sites and for the interstitial position, the latter being energetically less favored. Under S-rich conditions, it readily forms As_{Sn} in which case it acts as a donor. When the conditions are more Sn-rich, As_S becomes favorable in which case it acts as an acceptor. In this case, unlike the situation which occurs with Sb, the acceptor behavior of As_S is not significantly compensated by the As_{Sn} donor, which lies considerably higher in energy.

D. Highly electronegative defects: O and Cl

We next consider defects related either to the growth process itself or to interface layers in the photovoltaic device. In Fig. 5 we present the results for the highly electronegative elements Cl and O, which are found at high concentrations in SnS samples, as determined from mass spectroscopy experiments.[39] In experimental setups, gases such as $SnCl_4$[38] or other chlorine-containing precursors[40] are often used as source of Sn. SnS has also been grown epitaxially on NaCl substrates.[41] The sources of oxygen are the ambient environment, oxygen-containing growth precursors like those used in electrochemical deposition (ECD),[42] and substrates for SnS growth.[43] O has even been introduced intentionally in the growth environment to eliminate interface defects by oxidizing the SnS surface.[8,44]

We find that Cl has a strong energetic preference, under most experimental conditions and values of the Fermi level, to be a substitutional defect at the S site. In this position it acts as a single donor. This is in contrast to an experimental suggestion that Cl[38] impurities enhance the p-type nature of SnS. The Cl_{Sn} defect is an acceptor and has a very large formation enthalpy at values of the Fermi energy consistent with p-type behavior.

O strongly prefers to be incorporated into the SnS crystal as a S substitutional rather than as an interstitial or Sn substitutional, the latter possibility having very large formation enthalpy. This is in agreement with recent first-principles calculations which examined the role of oxygen passivation at the SnS surfaces.[44] The O_S defect is electrically inactive, and occurs in the neutral charge state for values of the Fermi level throughout the band gap.

E. Substrate-related defects: Na and Mo

Na and Mo are elements present in substrates on which SnS has been grown.[6,41] The calculated formation enthalpies for defects associated with the presence of Na and Mo atoms are shown in Fig. 6. Na is an element whose dominant effects strongly

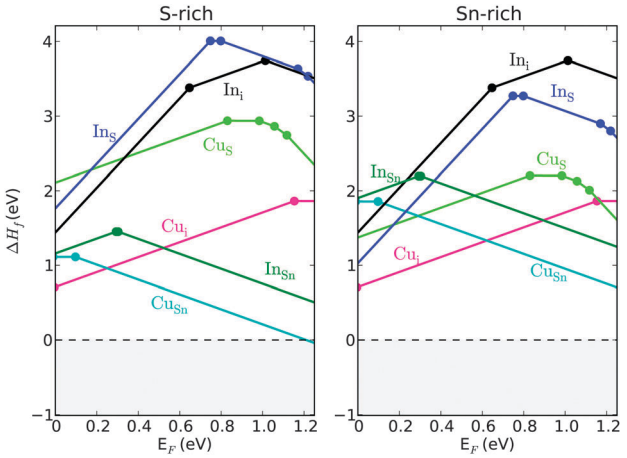

Fig. 7 Calculated defect formation enthalpies for extrinsic defects formed from the elements Cu and In, under S-rich (left) and Sn-rich (right) conditions.

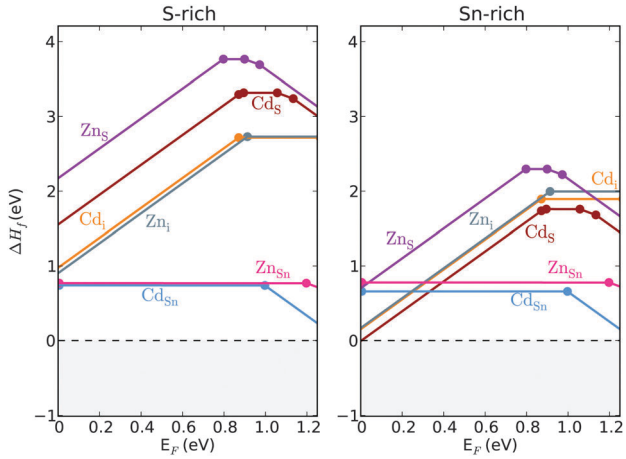

Fig. 8 Calculated defect formation enthalpies for extrinsic defects formed from the elements Zn and Cd, under S-rich (left) and Sn-rich (right) conditions.

depend on the experimental conditions. For example, under S-rich conditions the Na_{Sn} defect occurs with a very low formation enthalpy, in which case it acts as an acceptor. Under Sn-rich conditions, however, the situation is more complex, with the Na_i and Na_S defects becoming comparable in formation enthalpy to the Na_{Sn} defect, and both of them acting as donors.[45] The enthalpies of formation of Mo defects are generally higher than those of Na defects, although for certain values of the Fermi level the Mo_{Sn} and Mo_i defects have formation enthalpies less than 1 eV. In these configurations Mo acts as a donor with deep gap states which could possibly be detrimental to device performance.

F. d-electron elements: Cu, In, Zn, and Cd

Cu has been detected as an accidental impurity in SnS samples[36] and also has been deliberately introduced in order to tune the carrier concentration,[46] leading to an increase in the hole concentration. In has been considered as a dopant in a number of studies of SnS: in one such study, In is reported to increase the hole concentration[47] while in another study it has been reported to make SnS n-type, possibly by being a substitutional defect at the Sn site.[48]

Fig. 7 summarizes the results for the formation enthalpies for the defects that involve Cu and In atoms. These results show that Cu prefers to go into SnS as either an interstitial defect or as a substitutional defect at the Sn site. Under S-rich conditions, the Cu_{Sn} defect is the lowest enthalpy defect for most values of the Fermi level, acting as an acceptor. Under Sn-rich conditions, Cu can either act as a donor when the Fermi energy is low in the band gap, or as an acceptor when the Fermi energy is high.

All In defects have relatively high formation enthalpies (>1 eV) for Sn-rich conditions. Under S-rich conditions, the In_{Sn} defect can have relatively low formation enthalpy. This is in agreement with the experimental suggestion of ref. 48 that In forms substitutional defects at Sn sites. At high values of the Fermi energy it introduces holes into the material whereas for small values of the Fermi energy it compensates the existing holes by acting as a donor.

Zn and Cd are present in some of the common choices for n-type partners in SnS solar devices, such as ZnO, CdS, of $Cd_{1-x}Zn_xS$.[6] The enthalpies of defects associated with the presence of Zn and Cd atoms are shown in Fig. 8. These results show that Cd and Zn act in a very similar way as defects in SnS, a reasonable result due to their chemical similarity. The relative magnitudes of the formation enthalpies between the different defect sites for these two elements are quite close in most cases. Moreover, the placement and nature of the transitions between charge states of each defect are also quite similar for the two elements.

Under S-rich conditions Zn and Cd are electronically inactive: only the Sn substitutional defects have a reasonably low formation enthalpy and these are largely neutral through the entire range of Fermi energy values. Under Sn-rich conditions, however, the interstitial and S substitutional defects become energetically more favorable and these act primarily as donors. The electronic transition for the Sn substitutional is relatively shallow for Zn but is a little deeper in the gap for the corresponding Cd defect.

IV Conclusion

In this work we considered the role and nature of various intrinsic and extrinsic defects in bulk SnS, motivated by how their presence might affect on-going efforts to fabricate efficient solar cells utilizing SnS as an absorber layer. We performed first-principles calculations of the formation enthalpies of a large number of possible defects, using large 256-atom supercells in order to minimize finite-size effects. Additionally, in order to correct for spurious electrostatic interactions between periodic defect images, we use a recently developed scheme to properly account for the anisotropic nature of the screening.[27] In the process, we have also computed both the low-frequency and high-frequency dielectric constants from density functional perturbation theory. These values are in good agreement with prior experimental measurements and are, to our knowledge, the first theoretical results of these quantities, providing support for

Table 2 Summary of the dominant defects and their associated charge states, for the cases considered in this work under S-rich and Sn-rich conditions. The dominant defect, that is, the one with lowest formation enthalpy, and associated charge state are given separately for the "lower: region (0–0.3 eV), "mid-gap" region (0.3–0.95 eV), and "upper" region (0.95–1.25 eV) of the band gap of the pure crystal. V_X represents a vacancy of type X, where X = S or Sn; Y_X represents a substitutional atom of type Y, replacing an atom of type X. Positive charge states indicate donor behavior and negative charge states indicate acceptor behavior

	S-rich			Sn-rich		
	Lower	Mid-gap	Upper	Lower	Mid-gap	Upper
Intrinsic	$V_S(+2)$	$V_{Sn}(-2)$	$V_{Sn}(-2)$	$Sn_S(+4)$	$V_S(+2)$	$V_{Sn}(-2)$
P	$P_{Sn}(+1)$	$P_{Sn}(+1)$	$P_S(-1)$	$P_S(-1)$	$P_S(-1)$	$P_S(-1)$
N	$N_S(-1)$	$N_S(-1)$	$N_S(-1)$	$N_S(-1)$	$N_S(-1)$	$N_S(-1)$
As	$As_{Sn}(+1)$	$As_{Sn}(+1)$	$As_S(-1)$	$As_S(+0)$	$As_S(-1)$	$As_S(-1)$
Sb	$Sb_{Sn}(+1)$	$Sb_{Sn}(+1)$	$Sb_{Sn}(+1)$	$Sb_{Sn}(+1)$	$Sb_S(-1)$	$Sb_S(-1)$
Cl	$Cl_S(+1)$	$Cl_S(+1)$	$Cl_{Sn}(-3)$	$Cl_S(+1)$	$Cl_S(+1)$	$Cl_S(+1)$
O	$O_S(+0)$	$O_S(+0)$	$O_S(+0)$	$O_S(+0)$	$O_S(+0)$	$O_S(+0)$
Na	$Na_{Sn}(-1)$	$Na_{Sn}(-1)$	$Na_{Sn}(-1)$	$Na_{Sn}(-1)$	$Na_{Sn}(-1)$	$Na_{Sn}(-1)$
Mo	$Mo_{Sn}(+1)$	$Mo_{Sn}(+1)$	$Mo_{Sn}(-1)$	$Mo_i(+4)$	$Mo_{Sn}(+1)$	$Mo_{Sn}(-1)$
Cu	$Cu_i(+1)$	$Cu_{Sn}(-1)$	$Cu_{Sn}(-1)$	$Cu_i(+1)$	$Cu_{Sn}(-1)$	$Cu_{Sn}(-1)$
In	$In_{Sn}(+1)$	$In_{Sn}(-1)$	$In_{Sn}(-1)$	$In_S(+3)$	$In_{Sn}(-1)$	$In_{Sn}(-1)$
Zn	$Zn_{Sn}(+0)$	$Zn_{Sn}(+0)$	$Zn_{Sn}(+0)$	$Zn_i(+2)$	$Zn_{Sn}(+0)$	$Zn_{Sn}(+0)$
Cd	$Cd_{Sn}(+0)$	$Cd_{Sn}(+0)$	$Cd_{Sn}(-2)$	$Cd_S(+2)$	$Cd_{Sn}(+0)$	$Cd_{Sn}(-2)$

the infrared reflectivity and high-resolution electron-energy-loss spectroscopy measurements. For components of the dielectric tensor in which the experimental measurements show the most variability, our predicted result lies in between the experimental values.

A comprehensive summary of the dominant defect type for intrinsic defects and for each type of impurity considered, and the corresponding charge state of the dominant defect in each case, is given in Table 2. The results are shown separately for the lower (0–0.3 eV) region, the mid-gap (0.3–0.95 eV) and the upper (0.95–1.25 eV) region of the band gap of the pure SnS crystal.

For the intrinsic defects, we find a picture similar to that reported recently in ref. 13, namely that the energetically low-lying V_{Sn} acceptor defect is responsible for the intrinsic p-type conductivity of SnS. For the extrinsic defects, we make extensive comparison with experimental expectations of the nature of these defects. Our calculations shed new light on the role of the substrate in SnS photovoltaic devices. The Na_{Sn} acceptor occurs with very low formation energy and thus can work in tandem with the V_{Sn} intrinsic defect in making SnS p-type. Alternatively, Mo substrates do not contribute to p-type doping and might act to compensate some of the intrinsic p-type character, though the existence of deep transition states can introduce traps for carriers. Regarding the stability of SnS in air, an important characteristic for PV applications, we find that oxygen is not harmful as its low-energy defects are electrically inactive. We also find support for the interesting experimental suggestion that P, under S-rich conditions, prefers to substitutionally occupy the Sn site rather than the S site.[5] In this configuration P acts as a donor, providing theoretical evidence for the claim that by using P as a dopant in SnS nanowire arrays, n-type behavior can be obtained, which had proven difficult due to the apparent robust nature of the p-type conductivity in SnS. We find support for the experimental claim that Sb acts as a donor when introduced into SnS and that it is incorporated as Sb_{Sn} in a S-rich environment.[35] Other defects may also serve to increase the Fermi level in p-type SnS under various environments, including As_{Sn}, Cl_S, Mo_{Sn}, Na_i, Na_S, Cu_i, Cd_i, Cd_S, Zn_i, and Zn_S, providing avenues to further tune the carrier concentration of the SnS photovoltaic device.

Acknowledgements

We would like thank the members of the research groups of Prof. R. Gordon and T. Buonassisi for useful discussions, in particular Dr Prasert Sinsermsuksakul and Katy Hartman. AG acknowledges the support of the Lendület Program from the Hungarian Academy of Sciences. Computational resources were provided by the Extreme Science and Engineering Discovery Environment (XSEDE), supported by NSF grant number TG-DMR120073.

References

1 K. T. R. Reddy, N. K. Reddy and R. W. Miles, *Sol. Energy Mater. Sol. Cells*, 2006, **90**, 3041.
2 P. Sinsermsuksakul, J. Heo, W. Noh, A. S. Hock and R. G. Gordon, *Adv. Energy Mater.*, 2011, **1**, 1116.
3 R. W. Miles, O. E. Ogah, G. Zoppi and I. Forbes, *Thin Solid Films*, 2009, **517**, 4702.
4 K. Hartman, J. L. Johnson, M. I. Bertoni, D. Recht, M. J. Aziz, M. A. Scarpulla and T. Buonassisi, *Thin Solid Films*, 2011, **519**, 7421.
5 G. Yue, Y. Lin, X. Wen, L. Wang and D. Peng, *J. Mater. Chem.*, 2012, **22**, 16437.
6 P. Sinsermsuksakul, K. Hartman, S. B. Kim, J. Heo, L. Sun, H. H. Park, R. Chakraborty, T. Buonassisi and R. G. Gordon, *Appl. Phys. Lett.*, 2013, **102**, 053901.
7 H. Noguchi, A. Setiyadi, H. Tanamura, T. Nagatomo and O. Omoto, *Sol. Energy Mater. Sol. Cells*, 1994, **35**, 325.
8 P. Sinsermsuksakul, L. Sun, S. W. Lee, H. H. Park, S. B. Kim, C. Yang and R. G. Gordon, *Adv. Energy Mater.*, 2014, **4**, 1400496.
9 C. Wadia, A. P. Alivisatos and D. M. Kammen, *Environ. Sci. Technol.*, 2009, **43**, 2072.
10 L. Sun, R. Haight, P. Sinsermsuksakul, S. B. Kim, H. H. Park and R. G. Gordon, *Appl. Phys. Lett.*, 2013, **103**, 181904.
11 B. D. Malone and E. Kaxiras, *Phys. Rev. B: Condens. Matter Mater. Phys.*, 2013, **87**, 245312.
12 L. A. Burton and A. Walsh, *Appl. Phys. Lett.*, 2013, **102**, 132111.
13 J. Vidal, S. Lany, M. d'Avezac, A. Zunger, A. Zakutayev, J. Francis and J. Tate, *Appl. Phys. Lett.*, 2012, **100**, 032104.
14 G. Kresse and J. Hafner, *Phys. Rev. B: Condens. Matter Mater. Phys.*, 1993, **48**, 13115.
15 G. Kresse and J. Furthmüller, *Phys. Rev. B: Condens. Matter Mater. Phys.*, 1996, **54**, 11169.
16 G. Kresse and D. Joubert, *Phys. Rev. B: Condens. Matter Mater. Phys.*, 1999, **59**, 1758.

17 J. P. Perdew, K. Burke and M. Ernzerhof, *Phys. Rev. Lett.*, 1996, **77**, 3865.
18 H. Wiedemeier and H. G. von Schnering, *Z. Kristallogr.*, 1978, **148**, 295.
19 SnS has a layered crystal structure with space group D_{2h}^{16} containing 8 atoms in the primitive unit cell.
20 S. B. Zhang and J. E. Northrup, *Phys. Rev. Lett.*, 1991, **67**, 2339.
21 C. G. van de Walle and J. Neugenbauer, *J. Appl. Phys.*, 2004, **95**, 3851.
22 C. Persson, Y.-J. Zhao, S. Lany and A. Zunger, *Phys. Rev. B: Condens. Matter Mater. Phys.*, 2005, **72**, 035211.
23 R. Nieminen, *Modell. Simul. Mater. Sci. Eng.*, 2009, **17**, 084001.
24 N. D. M. Hine, K. Frensch, W. M. C. Foulkes and M. W. Finnis, *Phys. Rev. B: Condens. Matter Mater. Phys.*, 2009, **79**, 024112.
25 J. M. Chamberlain, P. M. Nikolić, M. Merdan and P. Mihailović, *J. Phys. C: Solid State Phys.*, 1976, **9**, L637.
26 S. Lany and A. Zunger, *Modell. Simul. Mater. Sci. Eng.*, 2009, **17**, 084002.
27 S. T. Murphy and N. D. M. Hine, *Phys. Rev. B: Condens. Matter Mater. Phys.*, 2013, **87**, 094111.
28 C. W. M. Castleton, A. Höglund and S. Mirbt, *Phys. Rev. B: Condens. Matter Mater. Phys.*, 2006, **73**, 035215.
29 M. S. Hybertsen and S. G. Louie, *Phys. Rev. B: Condens. Matter Mater. Phys.*, 1986, **34**, 5390.
30 P. Rinke, A. Janotti, M. Scheffler and C. G. Van de Walle, *Phys. Rev. Lett.*, 2009, **102**, 026402.
31 M. Gajdoš, K. Hummer, G. Kresse, J. Furthmüller and F. Bechstedt, *Phys. Rev. B: Condens. Matter Mater. Phys.*, 2006, **73**, 045112.
32 X. Wu, D. Vanderbilt and D. R. Hamann, *Phys. Rev. B: Condens. Matter Mater. Phys.*, 2005, **72**, 035105.
33 H. R. Chandrasekhar, R. G. Humphreys, U. Zwick and M. Cardona, *Phys. Rev. B: Solid State*, 1977, **15**, 2177.
34 L.-M. Yu, A. Degiovanni, P. A. Thiry, J. Ghijsen and R. Caudano, *Phys. Rev. B: Condens. Matter Mater. Phys.*, 1993, **47**, 16222.
35 P. Sinsermsuksakul, R. Chakraborty, S. B. Kim, S. M. Heald, T. Buonassisi and R. G. Gordon, *Chem. Mater.*, 2012, **24**, 4556.
36 W. Albers, C. Haas and F. van der Maesen, *J. Phys. Chem. Solids*, 1960, **15**, 306.
37 See ESI† for structural information surrounding each intrinsic defect, as obtained from the DFT relaxations.
38 A. Ortiz, J. C. Alonso, M. Garcia and J. Toriz, *Semicond. Sci. Technol.*, 1996, **11**, 243.
39 M. Parenteau and C. Carlone, *Phys. Rev. B: Condens. Matter Mater. Phys.*, 1990, 5227.
40 B. P. Bade, S. S. Garje, Y. S. Niwate, M. Afzaal and P. O'Brien, *Chem. Vap. Deposition*, 2008, **14**, 292.
41 A. Wangperawong, S. M. Herron, R. R. Runser, C. Hägglund, J. T. Tanskanen, H.-B.-R. Lee, B. M. Clemens and S. F. Bent, *Appl. Phys. Lett.*, 2013, **103**, 052105.
42 M. Ichimura, K. Takeuchi, Y. Ono and E. Arai, *Thin Solid Films*, 2000, **361**, 98.
43 N. R. Matthews, H. B. M. Anays, M. A. Cortes-Jacome, C. Angeles-Chavez and J. A. Toledo-Antonio, *J. Electrochem. Soc.*, 2010, **157**, H337.
44 G. A. Tritsaris, B. D. Malone and E. Kaxiras, *J. Appl. Phys.*, 2014, **115**, 173702.
45 The formation energy of the Na_{Sn} is similar under both S-rich and Sn-rich conditions, a coincidence caused by the effects of the competing phases on the allowed chemical potentials values as discussed in Section II.
46 S. Zhang and S. Cheng, *Micro Nano Lett.*, 2011, **6**, 559.
47 H. Weihui, C. Shuying and Z. Haifang, *ECS Trans.*, 2012, **44**, 1295.
48 M. Z. Sahdan, J. J. M. Vequizo, A. M. Abdel Haleem, M. Rusop and M. Ichimura, 2011 IEEE 2nd International Conference on Photonics (ICP), 2011, p. 1.